metals

MDPI

Article

Damping Characteristics of Inherent and Intrinsic Internal Friction of Cu-Zn-Al Shape Memory Alloys

Shyi-Kaan Wu [1], Wei-Jyun Chan [2] and Shih-Hang Chang [2,*]

[1] Department of Materials Science and Engineering, National Taiwan University, Taipei 106, Taiwan; skw@ntu.edu.tw

[2] Department of Chemical and Materials Engineering, National I-Lan University, I-Lan 260, Taiwan; r0423009@ms.niu.edu.tw

* Correspondence: shchang@niu.edu.tw; Tel.: +886-2-2363-7846

Received: 28 August 2017; Accepted: 22 September 2017; Published: 28 September 2017

Abstract: Damping properties of the inherent and intrinsic internal friction peaks (IF_{PT} + IF_I) of Cu-xZn-11Al (x = 7.0, 7.5, 8.0, 8.5, and 9.0 wt. %) shape memory alloys (SMAs) were investigated by using dynamic mechanical analysis. The Cu-7.5Zn-11Al, Cu-8.0Zn-11Al, and Cu-8.5Zn-11Al SMAs with $(IF_{PT} + IF_I)_{\beta_3(L2_1)\rightarrow\gamma_3'(2H)}$ peaks exhibit higher damping capacity than the Cu-7.0Zn-11Al SMA with a $(IF_{PT} + IF_I)_{\beta_3(L2_1)\rightarrow\gamma_3'(2H)}$ peak, because the γ_3' martensite phase possesses a 2H type structure with abundant movable twin boundaries, while the β_3' phase possesses an 18R structure with stacking faults. The Cu-9.0Zn-11Al SMA also possesses a $(IF_{PT} + IF_I)_{\beta_3(L2_1)\rightarrow\gamma_3'(2H)}$ peak but exhibits low damping capacity because the formation of γ phase precipitates inhibits martensitic transformation. The Cu-8.0Zn-11Al SMA was found to be a promising candidate for practical high-damping applications because of its high (IF_{PT} + IF_I) peak with tan δ > 0.05 around room temperature.

Keywords: shape memory alloys (SMAs); martensitic transformation; internal friction; dynamic mechanical analysis

1. Introduction

Shape memory alloys (SMAs) have been widely investigated for a broad range of applications because of their unique shape memory effect and superelasticity [1]. Numerous studies have shown that SMAs also exhibit a high damping capacity during martensitic transformation, and are effective for energy dissipation applications [2–5]. The damping capacity of SMAs is typically determined using an inverted torsion pendulum or dynamic mechanical analysis (DMA). During damping measurements, SMAs normally exhibit a significant internal friction peak (IF peak) at the martensitic transformation temperature, and the damping capacity is closely related to experimental parameters, including temperature rate, frequency, and applied strain amplitude [2,6].

The IF peak of SMAs typically comprises three individual terms (i.e., IF = IF_{Tr} + IF_{PT} + IF_I) [6–8]. IF_{Tr} denotes transient internal friction, which appears only at low frequencies and a non-zero temperature change rate. IF_{PT} is the inherent internal friction corresponding to phase transformation, which is independent of temperature rate. IF_I is the intrinsic internal friction of the austenitic or martensitic phase, and it depends strongly on microstructural properties such as dislocations, vacancies, and twin boundaries. It has been reported that IF_I is also temperature rate dependent, since time-dependent pinning affects the intrinsic damping and depends on the concentration of mobile pinning points throughout the heat treatment procedure during thermal cycling and deformation of Cu-based alloys [9–12]. The damping capacities of IF_{PT} and IF_I are usually more important than that of IF_{Tr} because most high-damping applications of SMAs are realized at a steady temperature.

Chang and Wu [13–22] have systematically studied the inherent and intrinsic internal friction (IF_{PT} + IF_I) peaks for various SMAs by applying DMA using the isothermal method. According to their results, TiNi-based SMAs exhibit acceptable damping capacities during martensitic transformations with tan $\delta > 0.02$. Cu-Al-Ni and Ni_2MnGa SMAs show (IF_{PT} + IF_I) peaks above room temperature. However, the damping capacity of the (IF_{PT} + IF_I) peaks for these SMAs was not as good as expected. The martensitic transformation temperatures of Cu-Zn-Al SMAs can be controlled by carefully adjusting their chemical composition [23], suggesting that Cu-Zn-Al SMAs have the potential to exhibit significant (IF_{PT} + IF_I) peaks above room temperature. Numerous studies have reported the transformation behaviors, crystal structures, and mechanical properties of Cu-Zn-Al SMAs [23–35]. Besides, several works in the literature have also investigated the internal friction properties of Cu-Zn-Al SMAs [36–40]. To date, the damping properties of (IF_{PT} + IF_I) peaks for Cu-Zn-Al SMA have not been investigated, to the best of our knowledge. Therefore, the aim of this study was to investigate the inherent and intrinsic internal friction properties of Cu-Zn-Al SMAs with regard to their damping properties.

2. Materials and Methods

Polycrystalline samples of Cu-xZn-11Al (x = 7.0, 7.5, 8.0, 8.5, and 9.0 wt. %) SMAs were prepared from pure copper (purity 99.9 wt. %), zinc (purity 99.9 wt. %), and aluminum (purity 99.9 wt. %). The raw materials were melted at 1100 °C in an evacuated quartz tube for 6 h and then slowly cooled in the furnace to room temperature to form Cu-xZn-11Al SMA ingots. The ingots were solution-treated at 850 °C for 12 h, followed by quenching in ice water. Each ingot was cut into bulks with dimensions of 30.0 mm × 6.0 mm × 3.0 mm for the DMA tests. The crystallographic features of the solution-treated Cu-xZn-11Al SMAs were determined using a Rigaku Ultima IV X-ray diffraction (XRD) instrument with Cu Kα radiation (λ = 0.154 nm) at room temperature. Microstructural observations of Cu-xZn-11Al SMAs were performed with a Tescan 5136MM scanning electron microscope (SEM). The chemical compositions of Cu-xZn-11Al SMAs were determined with an Oxford Instruments x-act energy-dispersive X-ray spectroscope (EDS). According to the EDS results, the determined chemical compositions for Cu-xZn-11Al with x = 7.0, 7.5, 8.0, 8.5, and 9.0 SMAs were Cu-7.14Zn-11.25Al, Cu-7.57Zn-11.29Al, Cu-8.18Zn-11.40Al, Cu-8.69Zn-10.91Al, and Cu-8.98Zn-10.83Al, respectively, suggesting that the determined chemical composition of each specimen was close to that of the expected composition. The martensitic transformation temperatures and the transformation enthalpy (ΔH) values for Cu-xZn-11Al SMAs were determined using a TA Q10 differential scanning calorimeter (DSC) under a constant cooling/heating rate of 10 $°C \cdot min^{-1}$. The damping capacity (tan δ) for Cu-xZn-11Al SMAs was determined using TA 2980 DMA equipment with a single cantilever clamp and a liquid nitrogen cooling apparatus. The parameters for the DMA tests were a temperature rate of 3 $°C \cdot min^{-1}$, frequency of 1 Hz, and strain amplitude of 1.0×10^{-4}. The inherent and intrinsic internal friction (IF_{PT} and IF_I) of Cu-xZn-11Al SMAs were also investigated by DMA, but tested under a temperature rate of 1 $°C \cdot min^{-1}$, frequency of 10 Hz, and strain amplitude of 1.0×10^{-4}.

3. Results and Discussion

3.1. XRD and SEM Results

Figure 1 presents the XRD results of Cu-xZn-11Al (x = 7.0, 7.5, 8.0, 8.5, and 9.0) SMAs. As shown in the figure, the Cu-7.0Zn-11Al SMA exhibits diffraction peaks at 2θ = 39.0°, 41.1°, 43.0°, 44.7°, 46.3°, and 47.8°, which correspond to the $(12\overline{2})$, (201), (0018), $(12\overline{8})$, (1210), and $(20\overline{10})$ diffraction planes, respectively, of the 18R structure [24]. Furthermore, the Cu-7.5Zn-11Al, Cu-8,0Zn-11Al, and Cu-8.5Zn-11Al SMAs exhibit diffraction peaks at 2θ = 40.0°, 42.7°, and 45.3°, which correspond to the (200), (002), and (201) diffraction planes, respectively, of the 2H structure [34]. The Cu-9.0Zn-11Al SMA shows only a sharp diffraction peak at 2θ = 43.2°, which corresponds to the (220) diffraction plane of the $L2_1$ structure. Therefore, we can conclude that the Cu-7.0Zn-11Al SMA is in the β'_3(18R) martensite phase at room temperature. On the other hand, the Cu-7.5Zn-11Al, Cu-8,0Zn-11Al, and

Cu-8.5Zn-11Al SMAs are in the γ'_3(2H) martensite phase, whereas the Cu-9.0Zn-11Al SMA is in the β_3(L2$_1$) parent phase at room temperature.

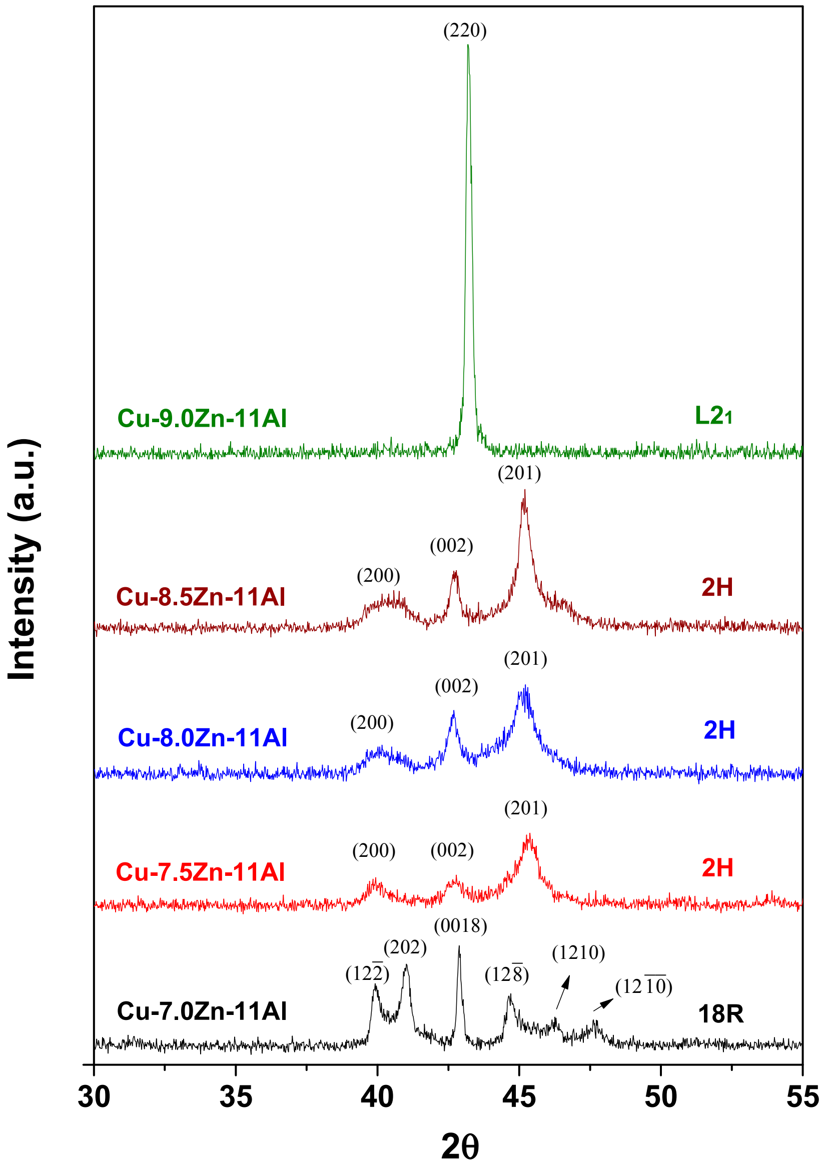

Figure 1. XRD patterns for Cu-xZn-11Al SMAs with various Zn contents.

Figure 2a–e shows the SEM images for the Cu-7.0Zn-11Al, Cu-7.5Zn-11Al, Cu-8.0Zn-11Al, Cu-8.5Zn-11Al, and Cu-9.0Zn-11Al SMAs, respectively. As shown in Figure 2a, the Cu-7.0Zn-11Al SMA exhibits typical self-accommodating, zig-zag groups of β'_3 martensite variants, indicating that it possesses an 18R structure at room temperature [33]. Figure 2b illustrates that the γ'_3(2H) martensite structure is dominant in the Cu-7.5Zn-11Al SMA. Figure 2c,d demonstrate that the Cu-8.0Zn-11Al and Cu-8.5Zn-11Al SMAs exhibit a γ'_3(2H) martensite phase at room temperature, where the γ'_3(2H) martensite plates become broader and more significant with the increase in Zn content. Figure 2e reveals that the Cu-9.0Zn-11Al SMA does not show obvious martensite variants because it adopts the β_3(L2$_1$) parent phase at room temperature. However, abundant γ phase precipitates appear along the grain boundaries of the alloy. This feature has also been reported by Condó et al. [31], wherein the γ phase normally formed when the electron/atom (e/a) ratios of Cu-Zn-Al SMAs were above 1.53.

Figure 2f depicts the magnification of the precipitates presented in Figure 2e and shows that the γ phase precipitates possess a typical crisscross structure with a size of approximately 20 µm.

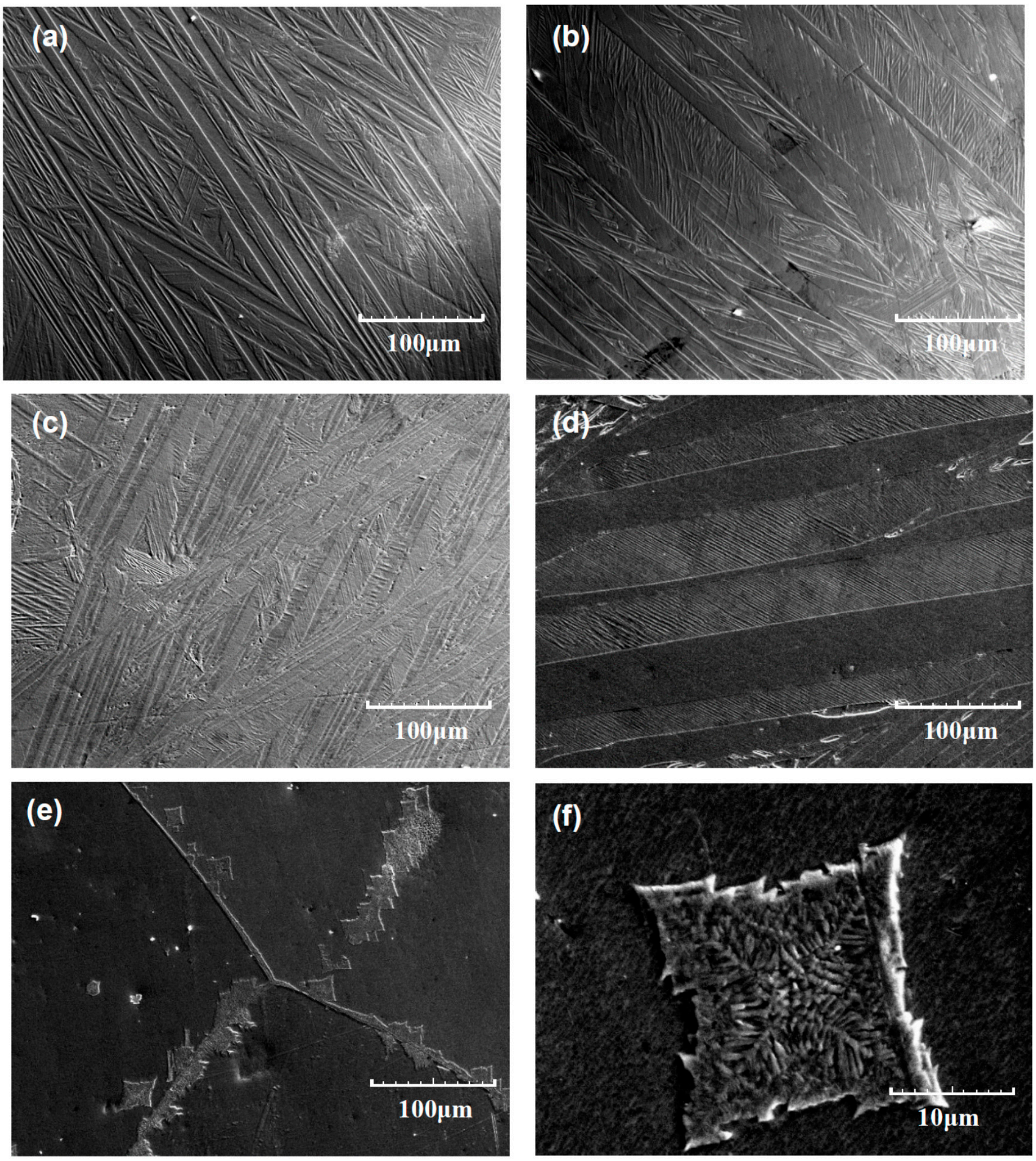

Figure 2. SEM images of (**a**) Cu-7.0Zn-11Al, (**b**) Cu-7.5Zn-11Al, (**c**) Cu-8.0Zn-11Al, (**d**) Cu-8.5Zn-11Al, and (**e**) Cu-9.0Zn-11Al SMAs under the same magnification. (**f**) A magnified SEM image of (**e**).

3.2. DSC Results

Figure 3 shows the DSC curves of Cu-xZn-11Al (x = 7.0, 7.5, 8.0, 8.5, and 9.0) SMAs. As shown in Figure 3, each Cu-xZn-11Al SMA exhibits a single martensitic transformation peak in both cooling and heating curves. According to the XRD and SEM results shown in Figures 1 and 2, one can conclude that the Cu-7.0Zn-11Al SMA possesses a β_3(L2$_1$) $\rightarrow$ β_3'(18R) martensitic transformation in cooling and a β_3'(18R) $\rightarrow$ (L2$_1$) transformation in heating. On the other hand, the Cu-7.5Zn-11Al, Cu-8.0Zn-11Al, and Cu-8.5Zn-11Al SMAs all exhibit a β_3(L2$_1$) $\rightarrow$ γ_3'(2H) martensitic transformation in cooling and a γ_3'(2H) $\rightarrow$ β_3(L2$_1$) transformation in heating. Although the Cu-9.0Zn-11Al SMA is in the β_3(L2$_1$) parent phase at room temperature, according to the report by Ahlers and Pelegrina [27], the Cu-9.0Zn-11Al SMA should also exhibit a β_3(L2$_1$) $\leftrightarrow$ γ_3'(2H) martensitic transformation, for its e/a value was calculated to be 1.528. Figure 3 also shows that the martensite start (Ms) temperature of the Cu-xZn-11Al SMAs decreases significantly from 104.0 °C to −21.2 °C when Zn content is increased from x = 7.0 to 9.0. This is consistent with the study reported by Ahlers [23], in which the Ms temperature of the Cu-Zn-Al SMA depended strongly on its chemical composition. On the other hand, the ΔH values of the specimens shown in Figure 3 are not significantly different, as all are close to 6 J/g.

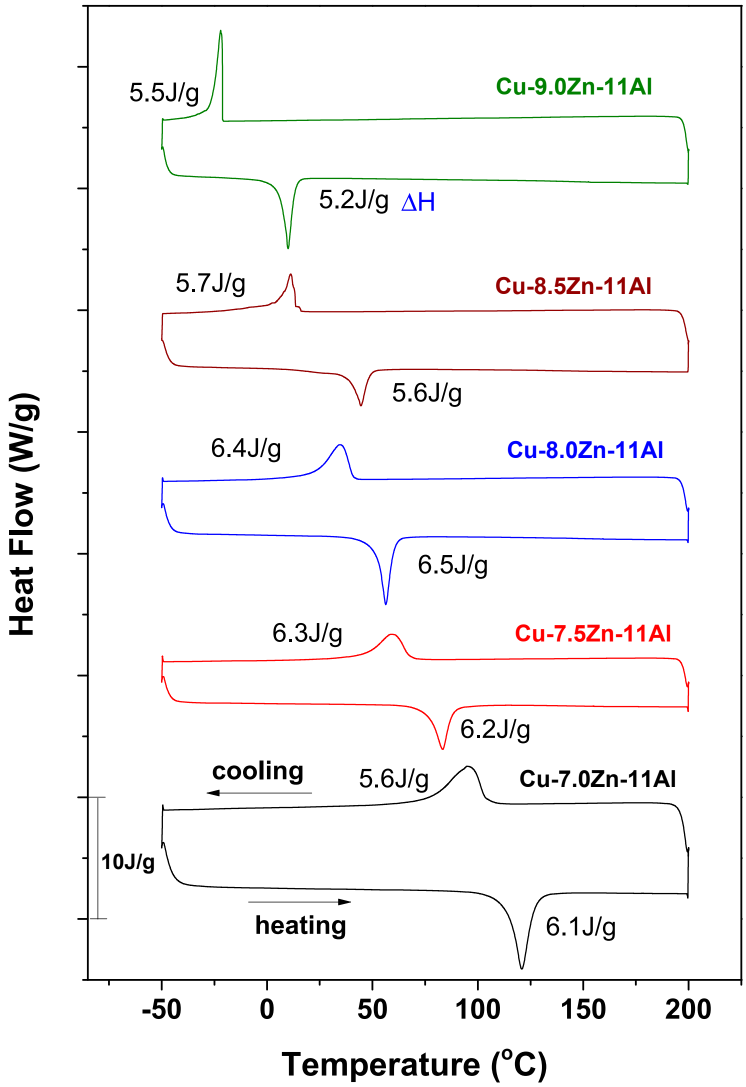

Figure 3. DSC curves for Cu-xZn-11Al SMAs with various Zn contents.

3.3. DMA Results

Figure 4 shows the DMA curves of Cu-xZn-11Al (x = 7.0, 7.5, 8.0, 8.5, and 9.0) SMAs measured at a controlled temperature rate of 3 °C·min^{-1}, frequency of 1 Hz, and strain amplitude of 1.0 × 10^{-4}. Only the DMA cooling curves are shown in Figure 4, for clarity. The Cu-7.0Zn-11Al SMA possesses a β_3(L2$_1$) → β'_3(18R) IF peak with tan δ = 0.065 at approximately 95.0 °C. Compared to the Cu-7.0Zn-11Al SMA, the Cu-7.5Zn-11Al, Cu-8.0Zn-11Al, and Cu-8.5Zn-11Al SMAs exhibit a more significant β_3(L2$_1$) → γ'_3(2H) IF peak with higher tan δ values, above 0.12. However, the IF peak temperatures for the Cu-7.5Zn-11Al, Cu-8.0Zn-11Al and Cu-8.5Zn-11Al SMAs were determined to be 59.8, 30.1, and −9.6 °C, respectively, which are much lower than that of the Cu-7.0Zn-11Al SMA. The Cu-9.0Zn-11Al SMA also possesses a β_3(L2$_1$) → γ'_3(2H) IF peak at approximately −11.4 °C; however, its tan δ value is only 0.082.

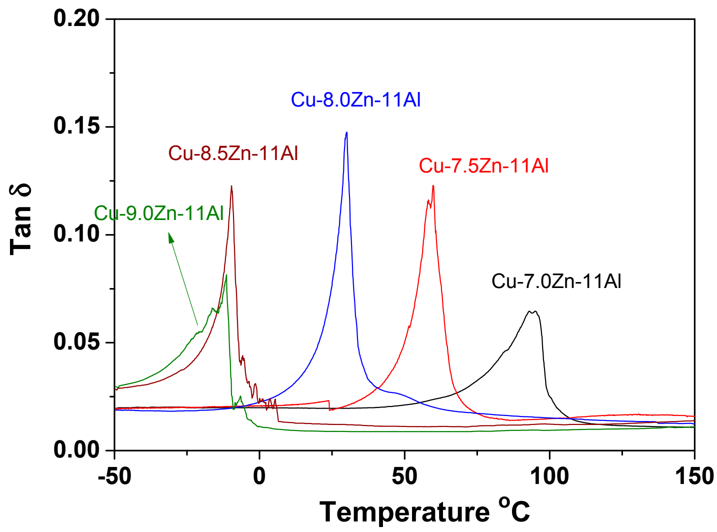

Figure 4. DMA tan δ curves measured at 1 Hz and 3 °C·min^{-1} cooling rate for Cu-xZn-11Al SMAs with various Zn contents.

3.4. IF_{PT} and IF_I Measurements

To investigate the inherent internal friction characteristics of Cu-xZn-11Al (x = 7.0, 7.5, 8.0, 8.5, and 9.0) SMAs, each specimen should be determined by DMA, but also assessed by the isothermal method reported previously [13]. A typical isothermal test-procedure can be described as follows: The SMA is initially cooled from the high temperature parent phase at a constant cooling rate and then maintained isothermally at a set temperature for a sufficient time interval to ensure that the IF_{Tr} term decays completely, leaving only the IF_{PT} and IF_I terms. Then, the SMA should be heated to a sufficiently high temperature to ensure that the SMA is completely in the parent phase state. Subsequently, the SMA is cooled to another set temperature and kept at a constant temperature to determine the IF_{PT} and IF_I values at that temperature. The aforementioned isothermal method can effectively and accurately determine the IF_{PT} and IF_I values of most SMAs [13–22]. However, this method is not suitable for the Cu-xZn-11Al SMAs in this study, because the repeated thermal cycling may influence the martensitic transformation properties of Cu-xZn-11Al SMAs, as demonstrated in Figure 5, which shows the DSC curve of the Cu-7.5Zn-11Al SMA for 10 repeated heating and cooling cycles. As per this figure, the Ms temperature of the Cu-7.5Zn-11Al SMA gradually decreased from 76.4 to 71.5 °C over the course of 10 repeated thermal cycles. In addition, the ΔH value of the Cu-7.5Zn-11Al SMA decreased from 6.3 J/g to 5.4 J/g. The decreasing Ms temperature and ΔH value can be attributed to the introduction of defects and dislocations during repeated thermal cycling, depressing the martensitic transformations of the Cu-7.5Zn-11Al SMA. Similar results were also observed in a previous study on the $Ti_{51}Ni_{39}Cu_{10}$ SMA [16].

To address this issue, the IF_{PT} and IF_I values for Cu-xZn-11Al SMAs were also determined by DMA, but the DMA was conducted at a high frequency where the IF_{Tr} term can be neglected [41]. In addition, Nespoli et al. [42] demonstrated that the IF values of SMAs determined by DMA at a 1 °C·min^{-1} cooling rate and 10 Hz frequency are very close to the IF_{PT} and IF_I determined under isothermal conditions. Accordingly, in this study, we used identical experimental parameters (1 °C·min^{-1} cooling rate and 10 Hz frequency) to determine the IF_{PT} and IF_I of Cu-xZn-11Al SMAs, and the results are presented in Figure 6. From Figure 6, it can be seen that the Cu-7.0Zn-11Al SMA possesses an inherent and intrinsic internal friction peak during the $\beta_3(\mathrm{L2_1}) \rightarrow \beta_3'(18\mathrm{R})$ martensitic transformation $(\mathrm{IF_{PT}} + \mathrm{IF_I})_{\beta_3(\mathrm{L2_1})\rightarrow\beta_3'(18\mathrm{R})}$ with tan δ = 0.026 at approximately 95.1 °C. Compared to the Cu-7.0Zn-11Al SMA, the Cu-7.5Zn-11Al SMA exhibited a higher $(\mathrm{IF_{PT}} + \mathrm{IF_I})_{\beta_3(\mathrm{L2_1})\rightarrow\gamma_3'(2\mathrm{H})}$ peak with a higher tan δ value of 0.040, but at a lower temperature of approximately 56.5 °C. Figure 6 also shows that both the Cu-8.0Zn-11Al and Cu-8.5Zn-11Al SMAs exhibit a high $(\mathrm{IF_{PT}} + \mathrm{IF_I})_{\beta_3(\mathrm{L2_1})\rightarrow\gamma_3'(2\mathrm{H})}$

peak with a tan δ value above 0.05 at approximately 32.2 and −6.8 °C, respectively. However, the Cu-9.0Zn-11Al SMA possesses a small $(\mathrm{IF_{PT}} + \mathrm{IF_I})_{\beta_3(\mathrm{L2_1})\rightarrow\gamma'_3(\mathrm{2H})}$ peak with tan δ = 0.030 at a low temperature of approximately −22.9 °C. In contrast to Figure 4, Figure 6 shows that the tan δ value of the ($\mathrm{IF_{PT}}$ + $\mathrm{IF_I}$) peak for each specimen measured at 10 Hz is much lower than that of the corresponding IF peak measured at 1 Hz, suggesting that the $\mathrm{IF_{Tr}}$ term disappears when Cu-xZn-11Al SMAs are measured at 10 Hz. Accordingly, we calculated the contribution of the ($\mathrm{IF_{PT}}$ + $\mathrm{IF_I}$) peak to the overall IF peak for each Cu-xZn-11Al SMAs, which was approximately 35% for all SMAs.

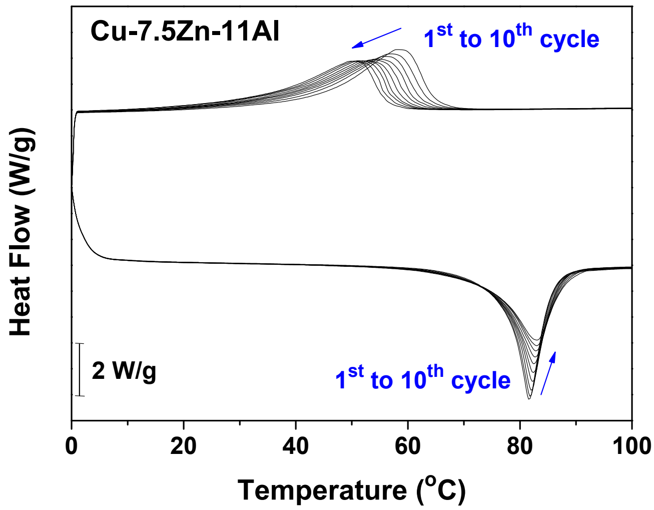

Figure 5. DSC curve of Cu-7.5Zn-11Al SMA determined for 10 repeating heating and cooling cycles.

Figure 6 also shows that the $(\mathrm{IF_{PT}} + \mathrm{IF_I})_{\beta_3(\mathrm{L2_1})\rightarrow\gamma'_3(\mathrm{2H})}$ peaks for the Cu-7.5Zn-11Al, Cu-8.0Zn-11Al, and Cu-8.5Zn-11Al SMAs (tan δ > 0.04) are much higher than that of $(\mathrm{IF_{PT}} + \mathrm{IF_I})_{\beta_3(\mathrm{L2_1})\rightarrow\beta'_3(\mathrm{18R})}$ for the Cu-7.0Zn-11Al SMA (tan δ = 0.026). In addition, the transformed γ'_3 martensite phases of the Cu-7.5Zn-11Al, Cu-8.0Zn-11Al, and Cu-8.5Zn-11Al SMAs possess a 2H type structure with abundant internal twin boundaries, which are easily moved to dissipate energy during damping [34]. On the other hand, the transformed β'_3 phase for the Cu-7.0Zn-11Al SMA only possesses an 18R structure with stacking faults, instead of movable twin boundaries [30]. Figure 6 reveals that the Cu-9.0Zn-11Al SMA also possesses an $(\mathrm{IF_{PT}} + \mathrm{IF_I})_{\beta_3(\mathrm{L2_1})\rightarrow\gamma'_3(\mathrm{2H})}$ peak during martensitic transformation, while exhibiting a lower tan δ value (0.030) compared to the other $(\mathrm{IF_{PT}} + \mathrm{IF_I})_{\beta_3(\mathrm{L2_1})\rightarrow\gamma'_3(\mathrm{2H})}$ peaks for Cu-xZn-11Al SMAs with lower Zn contents. This can be explained by the fact that abundant γ phase precipitates form in the Cu-9.0Zn-11Al SMA (Figure 2). These undesirable γ phase precipitates restrict the mobility of the parent phase/martensite interfaces, leading to a small $(\mathrm{IF_{PT}} + \mathrm{IF_I})_{\beta_3(\mathrm{L2_1})\rightarrow\gamma'_3(\mathrm{2H})}$ peak. Therefore, one can conclude that the Cu-8.0Zn-11Al SMA is more suitable for practical high-damping applications because of its high $(\mathrm{IF_{PT}} + \mathrm{IF_I})_{\beta_3(\mathrm{L2_1})\rightarrow\gamma'_3(\mathrm{2H})}$ peak with a tan δ value above 0.05 at around room temperature. However, according to the SEM results shown in Figure 2, the γ'_3(2H) martensite plates in Cu-xZn-11Al SMAs become broader with the increase in Zn content. Increasing the width of the martensite band normally decreases the number of twin boundaries, suggests that Cu-xZn-11Al SMAs with higher Zn content should exhibit lower damping capacity. Nevertheless, this is not seen in the DMA results shown in Figures 4 and 6. The reason for this unexpected DMA results is not clear yet, further follow-up studies will be carried out.

3.5. Comparison of the $\mathrm{IF_{PT}}$ and $\mathrm{IF_I}$ of the Cu-8.0Zn-11Al SMA with Other SMAs

According to our previous studies, $Ti_{50}Ni_{50}$ [13], $Ti_{50}Ni_{40}Cu_{10}$ [21], and $Ti_{50}Ni_{47}Fe_3$ [22] SMAs all have acceptable damping capacity, exemplified by their ($\mathrm{IF_{PT}}$ + $\mathrm{IF_I}$) peaks with tan δ > 0.02. However, their low martensitic transformation temperatures seriously restrict the use of these SMAs for practical high-damping applications. Although the Cu-14.0Al-4Ni SMA [20] exhibits an (IF_{PT} + IF_I) peak at approximately 70 °C, its damping capacity is extremely low. The group III Ni_2MnGa SMAs [18] exhibited good inherent internal friction, where tan $\delta > 0.02$, over a wide temperature range from −100 to 100 °C. However, the undesirable brittle nature of the Ni_2MnGa SMAs limited their workability and their use in high-damping applications. In this study, the Cu-8.0Zn-11Al SMA was shown to exhibit a high $(IF_{PT} + IF_I)_{\beta_3(L2_1)\rightarrow\gamma'_3(2H)}$ peak with a tan δ value above 0.053 at 32.2 °C. Except for the much higher (IF_{PT} + IF_I) peaks above room temperature, as compared to other SMAs, the Cu-Zn-Al SMAs also have better workability, lower cost, and acceptable mechanical properties, and desirable Ms temperatures can be obtained by adjusting the chemical composition of the alloys. Consequently, Cu-Zn-Al SMAs are promising high-damping materials under isothermal conditions.

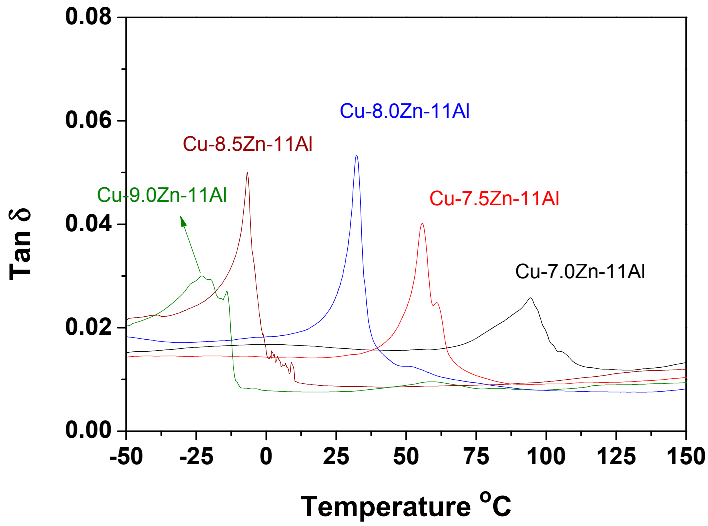

Figure 6. DMA tan δ curves measured at 10 Hz and 1 °C·min^{-1} cooling rate for Cu-xZn-11Al SMAs with various Zn contents.

4. Conclusions

Cu-xZn-11Al (x = 7.0, 7.5, 8.0, 8.5, and 9.0 wt. %) SMAs can exhibit a wide martensitic transformation temperature range from 104.0 to −21.2 °C by adjusting their chemical compositions. Cu-xZn-11Al SMAs with a higher ΔH value exhibit a higher IF peak because of the larger amount of martensite being transformed during martensitic transformation. The $(IF_{PT} + IF_I)_{\beta_3(L2_1)\rightarrow\gamma'_3(2H)}$ peaks for Cu-7.5Zn-11Al, Cu-8.0Zn-11Al, and Cu-8.5Zn-11Al SMAs are much higher than the $(IF_{PT} + IF_I)_{\beta_3(L2_1)\rightarrow\beta'_3(18R)}$ peak for the Cu-7.0Zn-11Al SMA because the transformed γ'_3 martensite phase possesses a 2H type structure with abundant movable twin boundaries, while the transformed β'_3 phase possesses an 18R structure with stacking faults. The Cu-9.0Zn-11Al SMA also possesses an $(IF_{PT} + IF_I)_{\beta_3(L2_1)\rightarrow\gamma'_3(2H)}$ peak during martensitic transformation; however, the abundant γ phase precipitates inhibit the movement of parent phase/martensite interfaces during damping, resulting in a lower tan δ value. The Cu-xZn-11Al SMAs are promising for practical high-damping applications under isothermal conditions because they possess good workability, low cost, acceptable mechanical properties, and the high damping capacities of the (IF_{PT} + IF_I) peaks around and above room temperature. Among them, Cu-8.0Zn-11Al SMA has a high (IF_{PT} + IF_I) peak with tan $\delta > 0.05$ appearing at ≈25 °C.

Acknowledgments: The authors gratefully acknowledge the financial support for this research provided by the Ministry of Science and Technology (MOST), Taiwan, under Grants MOST104-2221-E197-004-MY3 (S.-H. Chang) and MOST105-2221-E002-043-MY2 (S.-K. Wu).

Author Contributions: Wei-Jyun Chan contributed to the experimental procedures, results, and discussion sections of this paper. Shyi-Kaan Wu contributed to the results and discussion sections, and he is the principal investigator (PI) of the Grant MOST105-2221-E002-043-MY2. Shih-Hang Chang also contributed to the results and discussions sections, and he is the principal investigator of the Grant MOST 104-2221-E197-004-MY3. These grants are also mentioned in the Acknowledgement of this paper.

Conflicts of Interest: The authors declare no conflict of interest.

References

1. Otsuka, K.; Ren, X. Physical metallurgy of Ti-Ni-based shape memory alloys. *Prog. Mater. Sci.* **2005**, *50*, 511–678. [CrossRef]
2. Mercier, O.; Melton, K.N.; De Préville, Y. Low-frequency internal friction peaks associated with the martensitic phase transformation of NiTi. *Acta Metall.* **1979**, *27*, 1467–1475. [CrossRef]
3. Wu, S.K.; Lin, H.C.; Chou, T.S. A study of electrical resistivity, internal friction and shear modulus on an aged $Ti_{49}Ni_{51}$ alloy. *Acta Metall. Mater.* **1990**, *38*, 95–102. [CrossRef]
4. Coluzzi, B.; Biscarini, A.; Campanella, R.; Trotta, L.; Mazzolai, G.; Tuissi, A.; Mazzolai, F.M. Mechanical spectroscopy and twin boundary properties in a $Ni_{50.8}Ti_{49.2}$ alloy. *Acta Mater.* **1999**, *47*, 1965–1976. [CrossRef]
5. Fan, G.; Zhou, Y.; Otsuka, K.; Ren, X.; Nakamura, K.; Ohba, T.; Suzuki, T.; Yoshida, I.; Yin, F. Effects of frequency, composition, hydrogen and twin boundary density on the internal friction of $Ti_{50}Ni_{50-x}Cu_x$ shape memory alloys. *Acta Mater.* **2006**, *54*, 5221–5229. [CrossRef]
6. Bidaux, J.E.; Schaller, R.; Benoit, W. Study of the h.c.p.-f.c.c. phase transition in cobalt by acoustic measurements. *Acta Metall.* **1989**, *37*, 803–811. [CrossRef]
7. Van Humbeeck, J.; Stoiber, J.; Delaey, L.; Gotthardt, R. The high damping capacity of shape memory alloys. *Z. Metallkunde* **1995**, *86*, 176–183.
8. Dejonghe, W.; De Batist, R.; Delaey, L. Factors affecting the internal friction peak due to thermoelastic martensitic transformation. *Scr. Metall.* **1976**, *10*, 1125–1128. [CrossRef]
9. Kustov, S.; Golyandin, S.; Sapozhnikov, K.; Morin, M. Application of acoustic technique to determine the temperature range of quenched-in defect mobility in Cu-Al-Be β'_1 martensitic phase. *Scr. Mater.* **2000**, *43*, 905–911. [CrossRef]
10. Sapozhnikov, K.; Golyandin, S.; Kustov, S.; Van Humbeeck, J.; De Batist, R. Motion of dislocations and interfaces during deformation of martensitic Cu-Al-Ni crystals. *Acta Mater.* **2000**, *48*, 1141–1151. [CrossRef]
11. Sapozhnikov, K.; Golyandin, S.; Kustov, S.; Van Humbeeck, J.; Schaller, R.; De Batist, R. Transient internal friction during thermal cycling of Cu-Al-Ni single crystals in β'_1 martensitic phase. *Scr. Mater.* **2002**, *47*, 459–465. [CrossRef]
12. Kustov, S.; Golyandin, S.; Sapozhnikov, K.; Cesari, E.; Van Humbeeck, J.; De Batist, R. Influence of martensite stabilization on the low-temperature non-linear anelasticity in Cu-Zn-Al shape memory alloys. *Acta Mater.* **2002**, *50*, 3023–3044. [CrossRef]
13. Chang, S.H.; Wu, S.K. Inherent internal friction of B2 $\rightarrow$ R and R $\rightarrow$ B19′ martensitic transformations in equiatomic TiNi shape memory alloy. *Scr. Mater.* **2006**, *55*, 311–314. [CrossRef]
14. Chang, S.H.; Wu, S.K. Internal friction of R-phase and B19′ martensite in equiatomic TiNi shape memory alloy under isothermal conditions. *J. Alloys Compd.* **2007**, *437*, 120–126. [CrossRef]
15. Chang, S.H.; Wu, S.K. Internal friction of B2 $\rightarrow$ B19′ martensitic transformation of $Ti_{50}Ni_{50}$ shape memory alloy under isothermal conditions. *Mater. Sci. Eng. A* **2007**, *454–455*, 379–383. [CrossRef]
16. Chang, S.H.; Wu, S.K. Inherent internal friction of $Ti_{51}Ni_{39}Cu_{10}$ shape memory alloy. *Mater. Trans.* **2007**, *48*, 2143–2147. [CrossRef]
17. Chang, S.H.; Wu, S.K. Isothermal effect on internal friction of $Ti_{50}Ni_{50}$ alloy measured by step cooling method in dynamic mechanical analyzer. *J. Alloys Compd.* **2008**, *459*, 155–159. [CrossRef]
18. Chang, S.H.; Wu, S.K. Low-frequency damping properties of near-stoichiometric Ni_2MnGa shape memory alloys under isothermal conditions. *Scr. Mater.* **2008**, *59*, 1039–1042. [CrossRef]
19. Chang, S.H.; Wu, S.K. Determining transformation temperatures of equiatomic TiNi shape memory alloy by dynamic mechanical analysis test. *J. Alloys Compd.* **2013**, *577*, s241–s244. [CrossRef]
20. Chang, S.H. Influence of chemical composition on the damping characteristics of Cu-Al-Ni shape memory alloys. *Mater. Chem. Phys.* **2011**, *125*, 358–363. [CrossRef]
21. Chang, S.H.; Hsiao, S.H. Inherent internal friction of $Ti_{50}Ni_{50-x}Cu_x$ shape memory alloys measured under isothermal conditions. *J. Alloys Compd.* **2013**, *586*, 69–73. [CrossRef]

22. Chang, S.H.; Chien, C.; Wu, S.K. Damping characteristics of the inherent and intrinsic internal friction of $Ti_{50}Ni_{50-x}Fe_x$ (x = 2, 3, and 4) shape memory alloys. *Mater. Trans.* **2015**, *57*, 351–356. [CrossRef]
23. Ahlers, M. Martensite and equilibrium phases in Cu-Zn and Cu-Zn-Al alloys. *Prog. Mater. Sci.* **1986**, *30*, 135–186. [CrossRef]
24. Suzuki, T.; Kojima, R.; Fujii, Y.; Nagasawa, A. Reverse transformation behaviour of the stabilized martensite in Cu-Zn-Al alloy. *Acta Metall.* **1989**, *37*, 163–168. [CrossRef]
25. Tolley, A.; Rios Jara, D.; Lovey, F.C. 18R to 2H transformations in Cu-Zn-Al alloys. *Acta Metall.* **1989**, *37*, 1099–1108. [CrossRef]
26. Pelegrina, J.L.; Ahlers, M. The martensitic phases and their stability in Cu-Zn and Cu-Zn-Al alloys—I. The transformation between the high temperature β phase and the 18R martensite. *Acta Metall. Mater.* **1992**, *40*, 3205–3211. [CrossRef]
27. Ahlers, M.; Pelegrina, J.L. The martensitic phases and their stability in Cu-Zn and Cu-Zn-Al alloys—II. The transformation between the close packed martensitic phases. *Acta Metall. Mater.* **1992**, *40*, 3213–3220. [CrossRef]
28. Pelegrina, J.L.; Ahlers, M. The martensitic phases and their stability in Cu-Zn and Cu-Zn-Al alloys—III. The transformation between the high temperature phase and the 2H martensite. *Acta Metall. Mater.* **1992**, *40*, 3221–3227. [CrossRef]
29. Nakata, Y.; Yamamoto, O.; Shimizu, K. Effect of Aging in Cu-Zn-Al Shape Memory Alloys. *Mater. Trans. Jpn. Inst. Met.* **1993**, *34*, 429–437.
30. Saule, F.; Ahlers, M. Stability, stabilization and lattice parameters in Cu-Zn-Al martensites. *Acta Metall. Mater.* **1995**, *43*, 2373–2384. [CrossRef]
31. Condó, A.M.; Arneodo Larochette, P.; Tolley, A. Gamma phase precipitation processes in quenched beta phase Cu-Zn-Al alloys at an electron concentration of 1.53. *Mater. Sci. Eng. A* **2002**, *328*, 190–195. [CrossRef]
32. Arneodo Larochette, P.; Condó, A.M.; Pelegrina, J.L.; Ahlers, M. On the stability of the martensitic phases in Cu-Zn-Al, and its relationship with the equilibrium phases. *Mater. Sci. Eng. A* **2006**, *438–440*, 747–750. [CrossRef]
33. Asanović, V.; Delijić, K.; Jauković, N. A study of transformations of β-phase in Cu-Zn-Al shape memory alloys. *Scr. Mater.* **2008**, *58*, 599–601. [CrossRef]
34. Haberkorn, N.; Condó, A.M.; Espinoza, C.; Jaureguizahar, S.; Guimpel, J.; Lovey, F.C. Bulk-like behavior in the temperature driven martensitic transformation of Cu-Zn-Al thin films with 2H structure. *J. Alloys Compd.* **2014**, *591*, 263–267. [CrossRef]
35. Domenichini, P.; Condó, A.M.; Soldera, F.; Sirena, M.; Haberkorn, N. Influence of the microstructure on the resulting 18R martensitic transformation of polycrystalline Cu-Al-Zn thin films obtained by sputtering and reactive annealing. *Mater. Charact.* **2016**, *114*, 289–295. [CrossRef]
36. Zhao, Z.Q.; Chen, F.X.; Yang, D.Z. The internal friction associated with bainitic transformation, and bainitic transformation in a Cu-Zn-Al shape memory alloy. *J. Phys. Condens. Matter* **1989**, *1*, 1395–1404. [CrossRef]
37. Zhao, Z.Q.; Chen, F.X.; Li, S.Z.; Yang, D.Z. The internal friction associated with martensitic transformation in a CuZnAl shape memory alloy. *Scr. Metall. Mater.* **1991**, *25*, 669–672. [CrossRef]
38. Stoiber, J.; Bidaux, E.; Gotthardt, R. The movement of single $\beta_1 \rightarrow \beta_1'$ interfaces in Cu-Zn-Al as studied by a new technique of internal friction measurement. *Acta Metall. Mater.* **1994**, *42*, 4059–4070. [CrossRef]
39. Xiao, T.; Johari, G.P.; Mai, C. Time dependence of internal friction and shape change in Cu-Zn-Al shape memory alloys. *Metall. Trans. A* **1993**, *24*, 2743–2749. [CrossRef]
40. Cimpoeşu, N.; Stanciu, S.; Mayer, M.; Ioniţă, I.; Hanu Cimpoeşu, R. Effect of stress on damping capacity of a shape memory alloy CuZnAl. *J. Optoelectron. Adv. Mater.* **2010**, *12*, 386–391.
41. Perez-Saez, R.B.; Recarte, V.; No, M.L.; San Juan, J. Anelastic contributions and transformed volume fraction during thermoelastic martensitic transformations. *Phys. Rev. B* **1998**, *57*, 5684–5692. [CrossRef]
42. Nespoli, A.; Villa, E.; Passaretti, F. Quantitative evaluation of internal friction components of NiTiCu-Y shape memory alloys. *Thermochim. Acta* **2016**, *641*, 85–89. [CrossRef]